AIAA JOURNAL
Vol. 33, No. 12, December 1995

Euler-Based Inverse Method for Turbomachine Blades Part 1: Two-Dimensional Cascades

T. Dang* and V. Isgro*
Syracuse University, Syracuse, New York 13244-1240

A three-dimensional inverse method for the aerodynamic design of turbomachine blades using robust time-marching algorithms for the numerical solutions of the Euler equations is proposed. In this inverse method, the circumferential mass-averaged tangential velocity (or the blade loading) is the primary specified flow quantity, and the corresponding blade geometry is sought after. The presence of the blades is represented by a periodic array of discrete body forces which is included in the equations of motion. A four-stage Runge–Kutta time-stepping scheme is used to march a finite volume formulation of the unsteady Euler equations to a steady-state solution. Modification of the blade geometry during this time-marching process is achieved using the flow-tangency conditions along the blade surfaces. In this paper, the method is demonstrated for the design of two-dimensional infinitely thin cascaded blades ranging from the subsonic to the supersonic flow regimes, including cases with rotational flows and complex shock structures in the flow passage.

I. Background

DEVELOPMENT of turbomachinery blading with optimum aerodynamic efficiency has long been a design challenge. In the past, the problem was solved mostly by an approach which would depend on the past experience of the designers. The designers must have knowledge of how the blade geometry must be modified to achieve the desired performance. In more recent years, two-dimensional blade-to-blade inverse methodologies[1–5] have been developed and can now be employed to design blade profiles more readily. These inverse methods are based on the idea of specifying certain desired flow quantities and solving for the corresponding blade shape. Although these blade-to-blade inverse methods have been very useful design tools, the two-dimensional assumption is not accurate for turbomachine applications. Important flow phenomena that cannot be modeled by two-dimensional blade-to-blade methods include three-dimensional shock structures, secondary flows, and tip clearances.

Recently, a fully three-dimensional inverse method for the design of turbomachinery blading was proposed.[6–8] In this method, called the circulation method, the primary prescribed flow quantity is the pitch-averaged tangential velocity in the bladed region (related to the work distribution or the blade loading), and the calculated quantity is the three-dimensional blade geometry. The method has been successfully demonstrated for the design of infinitely thin blades in transonic flows,[9] viscous flows,[10] and blades with finite thickness.[11] Design studies for radial inflow turbines were carried out with this method, and the results were validated using existing Euler and Navier–Stokes computational fluid dynamics (CFD) analysis codes[12] and with an experimental verification program.[13]

In the circulation method, the classical aerodynamic approach of representing the blades as bound vortex sheets is adopted, and the equations of motion are cast in terms of Clebsch variables. As the majority of the existing analysis tools[14–16] are formulated in terms of conservative variables rather than Clebsch variables, we launched an investigation into the possibilities of reformulating the circulation method in terms of conservative variables. We have accomplished this goal by demonstrating the method in two dimensions using an existing time-marching algorithm for the Euler equations.

The principal idea in this newly developed inverse method consists of replacing the presence of the blades with a periodic discrete body-force field. This body-force field is included in the equations of motion, and an existing time-marching algorithm[17] is employed to integrate the finite volume formulation of the unsteady Euler equations to a steady-state solution. During this time-marching process, the blade geometry is modified using the flow-tangency boundary conditions along the blade surfaces.

II. Prescribed Quantities for Inverse Method

The conventional choices for the prescribed flow conditions in many blade-to-blade two-dimensional and quasi-three-dimensional inverse methods are the Mach number or pressure distributions along the blade pressure and suction surfaces.[1–3,5] These pressure distributions are chosen to avoid flow separation on the blade surfaces at the design condition. Strictly speaking, however, this design philosophy only applies to the two-dimensional case where it is known a priori that the streamlines along the blade surfaces lie in the two-dimensional plane under consideration. For three-dimensional flows, although this design philosophy may be adequate for external-flow applications such as the design of aircraft wings, it may not be satisfactory for internal-flow applications. The main reason is that in the flow passage of a turbomachine the potential presence of large radial velocities (i.e., secondary flows, tip-clearance flows) introduces excessive warping of a given stream surface across the blade passage. Thus, an accurate estimation of the locations of the blade-surface streamlines prior to a fully three-dimensional design calculation is a very difficult task. The other complication with this choice of prescribed flow quantity is the question of how arbitrarily one can specify the blade-surface pressure distributions at the different spanwise locations. It appears that certain criteria exist between the pressure distributions at the different spanwise stations, the simplest link being the radial-equilibrium condition.

In this study, the choice of prescribed quantities follows along the line of the general theory summarized in Tan et al.[8] for designing highly loaded blades in three dimensions. In this fully three-dimensional inverse method, the primary prescribed flow quantity is chosen to be the pitch-averaged fluid angular momentum per unit mass in the bladed region. This prescribed flow quantity, denoted by $r\bar{V}_\theta$, is defined as[8]

$$r\bar{V}_\theta(r,z) \equiv \frac{B}{2\pi}\int_0^{2\pi/B} rV_\theta(r,\theta,z)\,d\theta \tag{1}$$

where B is the number of blades. In two dimensions, the equivalent prescribed flow quantity is the pitch-averaged tangential velocity component, denoted by $\bar{V}_y$. This quantity is defined as

$$\bar{V}_y(x) \equiv \frac{1}{s}\int_0^s V_y(x,y)\,dy \tag{2}$$

where s is the blade spacing-to-chord ratio.

Received Sept. 7, 1994; revision received March 21, 1995; accepted for publication March 21, 1995.

*Department of Mechanical, Aerospace, and Manufacturing Engineering.

The pitch-averaged tangential velocity is a useful prescribed flow quantity because turbomachine blades supply energy or extract energy from a flowing fluid by imparting a change in the fluid's angular momentum about the axis of rotation. For the stator vanes, $\Delta(r\bar{V}_\theta)$ is the most appropriate quantity to prescribe because the function of these vanes in a turbomachine is to remove swirl (in a compressor) or add swirl (in a turbine) to the flow.

Once the overall change in the tangential velocity is established, the next task is to decide how to distribute this change in the bladed region. Novak and Haymann–Haber[4] and Tan et al.[8] have shown that the rate of change of the mean tangential velocity along the mean streamwise direction is related to the blade loading. Although the specification of the blade loading seems somewhat arbitrary, this type of design specification is used by many design offices in their throughflow methods,[18–20] and blade-to-blade inverse method.[4]

The other primary prescribed quantity in the circulation method is the blade thickness distribution.[11] The specification of the blade thickness distribution ensures that the designed blade is always closed. In addition, it allows for some control over the constraints set by structural and manufacturing requirements.

III. Theory

In this section, the theory is developed for infinitely thin blades and inviscid flows in two dimensions. The theory, however, is formulated so that it is readily extended to three dimensions and to include blade thickness[21] and three-dimensional viscous effects.[16]

A. Blade Body Force

In this proposed method, the infinitely thin blades are modeled by a discrete body-force field. The use of the body-force concept to model the presence of blade rows in turbomachine was first proposed by Marble[22] in axisymmetric flows. The concept of a distributed body-force field has been used extensively in throughflow methods.[18,19,23] This concept has also been used in conjunction with the time-marching techniques for 1) the three-dimensional Euler equations to model viscous effects in three-dimensions,[16] 2) the three-dimensional Navier–Stokes equations to model multistage effects in turbomachines,[14] and 3) the three-dimensional Euler equation combined with an actuator-disk model to study propeller/airframe flow interaction.[24] In this proposed method, we introduce the concept of a discrete body-force field to model the presence of a finite number of infinitely thin blades in a cascaded blade row.

We begin by noting two important characteristics of the blade body-force field. First, the blade body force must be zero everywhere except at the blades. Second, the blade body force must point in the direction normal to the blade surface since it represents entirely the reaction on the fluid of ideal pressure forces on the blades.[22] When using these two properties, the blade-body force field can be expressed as

$$\boldsymbol{F}_B \equiv \delta_p(\alpha) A \nabla\alpha \tag{3}$$

In Eq. (3), the blade surfaces as described by the function α are given by (Fig. 1)

$$\alpha \equiv y - f(x) = ns \tag{4}$$

where n is an integer. For homenthalpic and homentropic flows, Dang and Isgro[25] show that $A = A(x)$ can be related to the prescribed flow quantity $\bar{V}_y$ via Crocco's equation,

$$A(x) = \boldsymbol{V}_{\text{bl}} \bullet \nabla \bar{V}_y \tag{5}$$

where the blade velocity $\boldsymbol{V}_{\text{bl}}$ is defined as the average velocity between the blade upper and lower surfaces

$$\mathbf{V}_{\text{bl}} \equiv \tfrac{1}{2}(\boldsymbol{V}^+ + \boldsymbol{V}^-) \tag{6}$$

Hence, the blade body force takes on the form

$$\boldsymbol{F}_B = \delta_p(\alpha)[\boldsymbol{V}_{\text{bl}} \bullet \nabla \bar{V}_y]\nabla\alpha \tag{7}$$

The expression for the blade body force given in Eq. (7) is valid for the special case of homenthalpic and homentropic flows only.

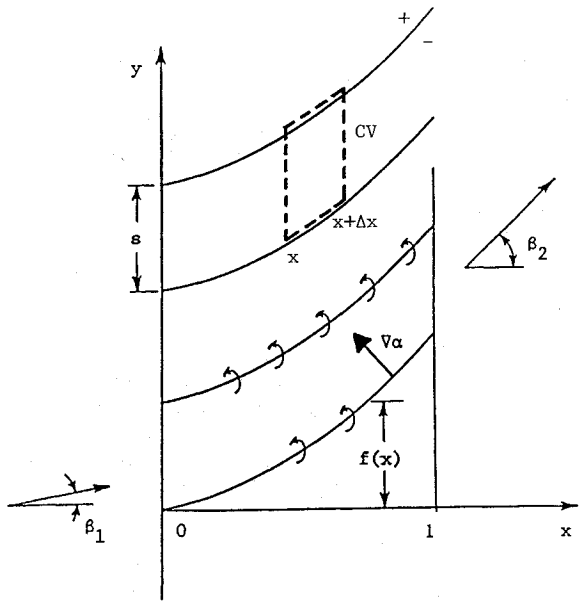

Fig. 1 Cascade notation.

For general rotational flows, the blade body force still takes on the form given in Eq. (3), but its strength as described by the function $A(x)$ given in Eq. (5) needs to be modified.

The function $A(x)$ can be related to the local flow by considering the y-momentum equation for a control volume enclosing the blade passage (Fig. 1). On using the flow-tangency condition at the blade surfaces along with the periodicity condition, the y-momentum equation applied to this control volume yields

$$\Delta x \int_0^s \rho(\boldsymbol{F}_B \bullet \hat{e}_y)\,\mathrm{d}y = \left[\int_0^s V_y(\rho V_x\,\mathrm{d}y)\right]_{x+\Delta x} - \left[\int_0^s V_y(\rho V_x\,\mathrm{d}y)\right]_x \tag{8}$$

Substituting the general expression for the blade body force given in Eq. (3) into Eq. (8), we obtain

$$A(x) = \frac{1}{s}\frac{1}{\rho_{\text{bl}}}\frac{\mathrm{d}}{\mathrm{d}x}\left[\int_0^s V_y(\rho V_x\,\mathrm{d}y)\right] \tag{9}$$

We define the circumferential mass-averaged tangential velocity, denoted by $\hat{V}_y = \hat{V}_y(x)$, as

$$\hat{V}_y(x) \equiv \frac{1}{\dot{m}}\int_0^s V_y(\rho V_x\,\mathrm{d}y) \tag{10}$$

Using the Eq. (10) definition of $\hat{V}_y$, the blade body force takes on the form

$$\boldsymbol{F}_B = \delta_p(\alpha)\left(\frac{\dot{m}}{s\rho_{\text{bl}}}\frac{\mathrm{d}\hat{V}_y}{\mathrm{d}x}\right)\nabla\alpha \tag{11}$$

B. Equations of Motion

The equations to be solved here are the unsteady Euler equations expressed in terms of the conservative variables, namely,

$$\frac{\partial \boldsymbol{U}}{\partial t} + \frac{\partial \boldsymbol{E}}{\partial x} + \frac{\partial \boldsymbol{F}}{\partial y} = \boldsymbol{H} \tag{12}$$

In Eq. (12), $\boldsymbol{U}$ is the conservative-variable vector and $\boldsymbol{E}$ and $\boldsymbol{F}$ are the inviscid flux vectors defined as

$$\boldsymbol{U} = \begin{Bmatrix} \rho \\ \rho V_x \\ \rho V_y \\ E_t \end{Bmatrix} \quad \boldsymbol{E} = \begin{Bmatrix} \rho V_x \\ \rho V_x^2 + p \\ \rho V_y V_x + p \\ (E_t + p)V_x \end{Bmatrix} \quad \boldsymbol{F} = \begin{Bmatrix} \rho V_y \\ \rho V_x V_y \\ \rho V_y^2 + p \\ (E_t + p)V_y \end{Bmatrix} \tag{13}$$

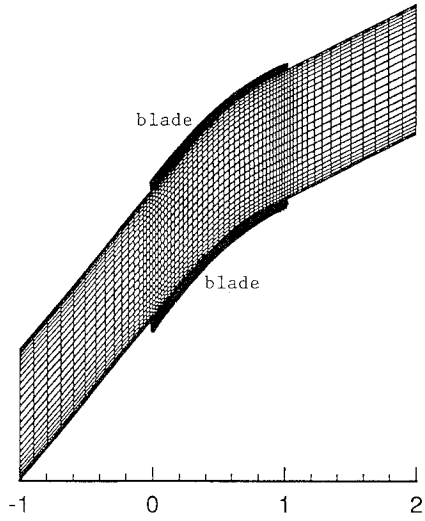

Fig. 2 Computational domain.

and $\boldsymbol{H}$ is the source vector which models the presence of the blades. On using Eq. (11), the source vector $\boldsymbol{H}$ takes on the form

$$\boldsymbol{H} = \begin{Bmatrix} 0 \\ \rho \boldsymbol{F}_B \bullet \hat{e}_x \\ \rho \boldsymbol{F}_B \bullet \hat{e}_y \\ 0 \end{Bmatrix} = \delta_p(\alpha) \left(\frac{\dot{m}}{s} \frac{\mathrm{d}\hat{V}_y}{\mathrm{d}x} \right) \begin{Bmatrix} 0 \\ -\dfrac{\mathrm{d}f}{\mathrm{d}x} \\ 1 \\ 0 \end{Bmatrix} \tag{14}$$

Conceptually, the difference in the flow equations between a standard analysis method and the present inverse method is the presence of the source term given in Eq. (14). Since the source term is zero everywhere except at the blades, however, we choose a computational domain that excludes the blade camber lines so that the source term $\boldsymbol{H}$ vanishes (Fig. 2). With this choice of computational domain, the presence of the blade body force in the equations is replaced by the implementation of a pressure-jump condition across the blade camber line. This condition can be derived by considering an infinitely thin control volume enclosing the blade camber line of axial length Δx. On using the flow-tangency condition along the blade surfaces, the y-momentum equation applied to this control volume reads

$$(p^- - p^+) + \int \rho(\boldsymbol{F}_B \bullet \hat{e}_y)\, \mathrm{d}y = 0 \tag{15}$$

Substituting the expression for the blade body force given in Eq. (11) into Eq. (15), the pressure-jump condition across the blade camber line is obtained:

$$\Delta p \equiv p^+ - p^- = \dot{m} \frac{\mathrm{d}\hat{V}_y}{\mathrm{d}x} \tag{16}$$

Equation (16) is the well-known relation between the blade pressure loading and the circumferential mass-averaged tangential velocity $\hat{V}_y$.

C. Camber Line Generator

In the inverse mode, the flow-tangency condition along the blade surface is replaced by a pressure-jump boundary condition in solving Eq. (12). We use the flow-tangency condition to update the blade camber line. The mathematical statements of the flow-tangency conditions along the blade upper and lower surfaces are

$$\boldsymbol{V}^{\pm} \bullet \nabla \alpha = 0 \tag{17}$$

Adding relations (17) and using Eq. (4) yields an initial-value ordinary differential equation (ODE) problem for the camber line function f

$$\frac{\mathrm{d}f}{\mathrm{d}x} = \frac{V_{\mathrm{bl},y}}{V_{\mathrm{bl},x}} \tag{18}$$

Given the velocities along the blade upper and lower surfaces, this equation can be integrated in the axial direction to obtain the blade camber line f. In the present method, Eq. (18) is integrated from the blade leading edge ($x = 0$) to the blade trailing edge ($x = 1$), with the arbitrarily chosen condition $f = 0$ at the blade leading edge. Note that in three-dimensional flows, the boundary condition for f constitutes the blade stacking condition.[8]

D. Formulation of Inverse Problem

In the proposed inverse method, the circumferential mass-averaged tangential velocity distribution $\hat{V}_y(x)$ in the bladed region (or the blade loading) is prescribed, and the blade camber line $f(x)$ is calculated. We note that the specification of $\hat{V}_y$ is subjected to the Kutta condition, which states that the pressure difference across the blade trailing edge must be zero. Equation (16) implies that $\mathrm{d}\hat{V}_y/\mathrm{d}x$ must vanish at the blade trailing edge to satisfy the Kutta condition. The calculation of the blade shape consists of periodically updating the blade camber line $f(x)$ using Eq. (18) during the time-marching process of the unsteady Euler equations to steady state.

IV. Numerical Technique

In the inverse problem, every time the blade shape is updated during the time-marching process, a new computational mesh needs to be generated. To alleviate the grid generation task, the simple sheared H grid topology is employed (Fig. 2). This choice of grid topology reduces to the need to generate the mesh in the (x, α) plane only once at the beginning of the inverse calculation. This mesh is a simple rectangular mesh since $0 \leq \alpha \leq s$. During the iteration process for the blade camber line $f(x)$, the y coordinate is updated using Eq. (4), namely,

$$y_{i,j} = \alpha_{i,j} + f_i \tag{19}$$

where $\alpha_{i,j}$ is fixed and f_i varies during the iteration process for the blade shape.

A. Flow Solver

The unsteady Euler equation is marched to steady state using the cell-centered finite volume Runge–Kutta time-stepping scheme proposed by Jameson et al.[17] This scheme consists of discretizing the integral form of Eq. (12) using a finite volume technique which reduces to a centered-difference approximation on a uniform square grid. Blended nonlinear second- and fourth-difference artificial dissipations are needed to prevent oscillations in the numerical solutions. The resulting system of ODEs is then integrated using a four-stage Runge–Kutta time-stepping scheme. The details of this algorithm are not given here and can be found in Jameson et al.[17] We note that no convergence-acceleration technique is implemented in our computer code.

B. Boundary Conditions

The standard method of imposing boundary conditions based on the theory of incoming and outgoing characteristic waves is adopted here. In the case of subsonic inflow, we specify $\{P_{01}, T_{01}, \beta_1\}$, and we extrapolate the static pressure p_1. In the case of supersonic inflow, we specify $\{P_{01}, T_{01}, \beta_1, M_1\}$. In the case of subsonic outflow, we specify the exit static pressure p_2, and we extrapolate for the remaining three primitive variables. Finally, in the case of supersonic outflow, we extrapolate all four primitive variables.

Outside the bladed region, the usual periodic boundary condition is applied along the upper and lower boundaries. In the bladed region, the flow-tangency conditions on the blade surfaces are not enforced in the inverse mode. Instead, a pressure-jump condition is imposed across the blade surfaces, and fluid is allowed to cross the blade surfaces during the iteration process for the blade camber line. This type of "permeable" boundary condition through a solid boundary during the transient calculation has been used in earlier studies[6–9] and in the two-dimensional inverse method recently proposed by Leonard and Van den Braembussche.[2] The flow-tangency conditions along the blade surfaces are used to update the blade shape via the camber line generator [Eq. (18)]. Consequently, when

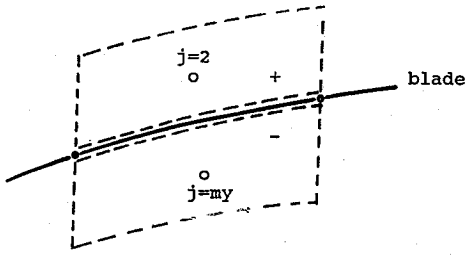

Fig. 3 Computational cells located above and below blade.

the solution converges, the blade camber line is successfully adjusted so that the flow is tangent to the blade surfaces, and the flow-tangency conditions on the blade surfaces are satisfied.

In the present cell-centered finite volume formulation, the technique used to evaluate the fluxes for the computational cells located along the upper and lower boundaries is as follows. In the bladed region, the computational cells along the lower boundary are chosen to be located just above the blade (cell $j = 2$ shown in Fig. 3), whereas the computational cells along the upper boundary are chosen to be located just below the blade (cell $j = my$ shown in Fig. 3). For these cells, we propose the following procedure for the inverse problem to evaluate the fluxes at the cell faces adjacent to the blades. The density and the velocity components are taken to be the blade values, namely,

$$\rho_{\text{bl}} \equiv \tfrac{1}{2}(\rho^+ + \rho^-) = \tfrac{1}{2}(\rho_{i,j=2} + \rho_{i,j=my}) \tag{20}$$

$$\boldsymbol{V}_{\text{bl}} \equiv \tfrac{1}{2}(\boldsymbol{V}^+ + \boldsymbol{V}^-) = \tfrac{1}{2}(\boldsymbol{V}_{i,j=2} + \boldsymbol{V}_{i,j=my}) \tag{21}$$

For the pressure, we need to be consistent with the pressure-jump condition given in Eq. (16). This condition is satisfied by evaluating the pressure force along the cell faces adjacent to the upper and lower surfaces as follows:

$$p^{\pm} \equiv p_{\text{bl}} \pm \frac{\dot{m}}{2}\frac{\mathrm{d}\hat{V}_y}{\mathrm{d}x} \tag{22}$$

where

$$p_{\text{bl}} \equiv \tfrac{1}{2}(p^+ + p^-) = \tfrac{1}{2}(p_{i,j=2} + p_{i,j=my}) \tag{23}$$

Clearly, when the solution converges, the flow is aligned with the blade profile, and the only contributions in the flux vectors $\boldsymbol{E}$ and $\boldsymbol{F}$ at the cell faces adjacent to the blades are the pressure forces. Consequently, averaging the density and the velocity components at the cell faces adjacent to the blade will not cause any numerical errors since the mass, momentum, and energy fluxes are all zeros at these cell boundaries when the solution converges.

A computer program written in both the analysis and inverse modes was developed. In terms of coding, the primary difference between the analysis mode and the inverse mode is in the subroutine used to evaluate the fluxes at the cell faces next to the blades. In the analysis mode, the flow-tangency condition is imposed at these cell faces, whereas in the inverse mode, a pressure-jump condition is imposed at these cell faces. In addition, in the inverse mode, the blade shape along with the computational mesh is periodically updated during the time-marching process.

V. Results

The first example presented is the design of a compressor blade in the subsonic-flow regime. The computational mesh has 64 cells in the streamwise direction and 24 cells in the pitchwise direction (Fig. 2). The blade spacing-to-chord ratio s is chosen to be unity, the inflow angle is taken to be 50 deg, and the back pressure is set at 0.85 (normalized to $\bar{P}_{01}$). The prescribed blade loading shape is a parabolic profile of the form

$$\frac{\mathrm{d}\hat{V}_y}{\mathrm{d}x} = 6\Delta\hat{V}_y x(1-x) \tag{24}$$

which has the maximum loading located at midchord. In the present design, the overall change in the circumferential mass-averaged tangential velocity $\Delta\hat{V}_y$ is set at -0.40 [normalized to $(R\bar{T}_{01})^{1/2}$]. Note

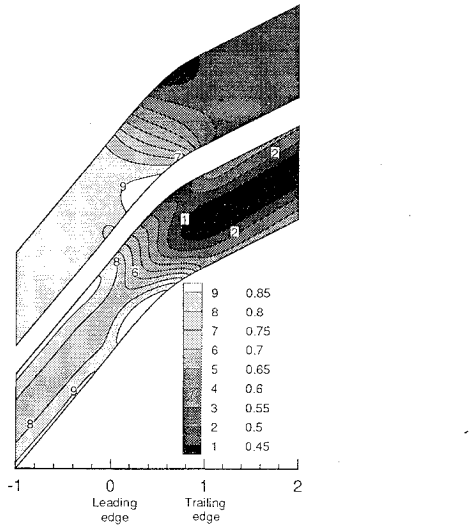

Fig. 4 Comparison of Mach number contour: irrotational flow at top of figure and rotational flow at bottom of figure.

that the blade pressure loading given in Eq. (24) vanishes at the blade leading edge ($x = 0$) and trailing edge ($x = 1$). Hence, it enforces the zero-incidence condition at the leading edge and satisfies the Kutta condition at the trailing edge.

Both irrotational and rotational upstream flows are considered in this example. For the latter case, the upstream circumferential variations in the stagnation pressure and stagnation temperature are taken to be of the form

$$\frac{P_{01}(y)}{\bar{P}_{01}} = 1 + \frac{\Delta P_{01}}{\bar{P}_{01}}\cos\left(2\pi\frac{y}{s}\right) \tag{25}$$

$$\frac{T_{01}(y)}{\bar{T}_{01}} = 1 + \frac{\Delta T_{01}}{\bar{T}_{01}}\cos\left(2\pi\frac{y}{s}\right) \tag{26}$$

where $\Delta P_{01}/\bar{P}_{01} = 0.05$ and $\Delta T_{01}/\bar{T}_{01} = -0.05$.

Figure 4 illustrates the Mach number contours about the designed blade passages. The top contour plot corresponds to the irrotational-flow case, whereas the bottom contour plot corresponds to the rotational-flow case. The Mach number in the flowfield ranges from 0.45 to 0.85 for these two subsonic-flow designs. It is interesting to note that the designed blade profiles in the irrotational- and rotational-flow cases are very similar.

Next, the analysis mode of the present code is used to verify the solutions given by the inverse mode. To carry out this consistency check, the flowfields through the blade passages designed using the inverse mode of the code are analyzed using the analysis mode of the code. The first consistency check is to confirm that the designed blade profiles do produce the prescribed $\hat{V}_y$ distribution given in Eq. (24). Figure 5 illustrates excellent comparisons of the $\hat{V}_y$ distribution between the prescribed values (solid line) and the values given by the analysis method (circle symbol). The distribution of $\hat{V}_y$ in the analysis mode is computed from the numerical solution using the definition given in Eq. (10). A more difficult consistency check is the comparison of the local flow variables such as the Mach number distribution on the blade surfaces. Figure 6 shows excellent comparisons of the blade surface Mach number distributions given by the inverse method (solid line) and the analysis method (circle symbol).

The next example concerns the design of supersonic throughflow (STF) fans. In a STF blade design, the axial component of the velocity remains supersonic throughout the blade row. In this study, the STF blades are designed using the following uniform inflow conditions. The inflow Mach number is chosen to be 2.0, and the inflow angle is taken to be 20 deg. The blade spacing-to-chord ratio s is chosen to be 0.35, and the blades are to be designed such that the flow leaving the blades has zero swirl (i.e., $\hat{V}_{y2} = 0$). Using these prescribed inflow conditions, the overall change in the normalized circumferential mass-averaged tangential velocity $\Delta\hat{V}_y$ can be

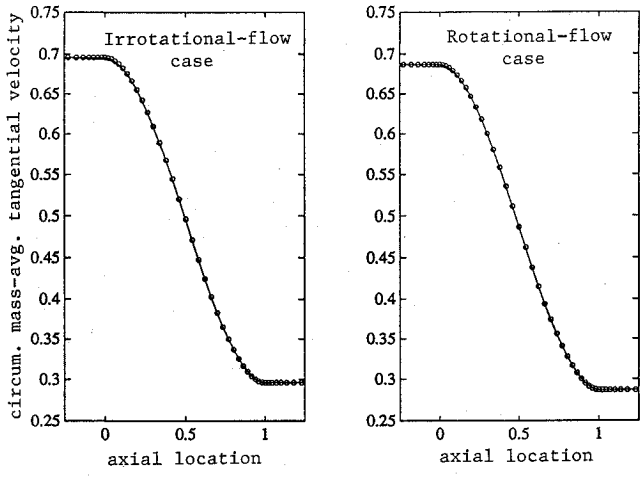

Fig. 5 Comparison of $\hat{V}_y(x)$: inverse mode is solid line and analysis mode is circle symbol.

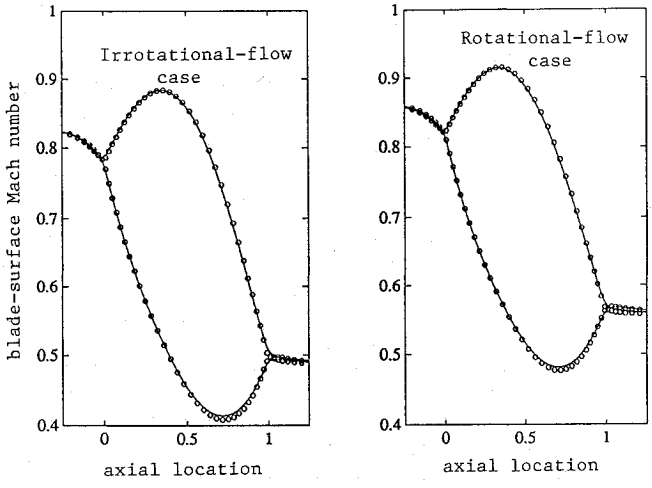

Fig. 6 Comparison of blade-surface Mach number: inverse mode is solid line and analysis mode is circle symbol.

shown to be −0.603. Finally, the computational mesh has 136 cells in the streamwise direction and 24 cells in the pitchwise direction.

To demonstrate the usefulness of this inverse method, we begin this design study by intentionally choosing a poorly designed initial blade profile, followed by an attempt to improve the design using the proposed inverse method. The initial blade profile is generated using the "conventional" approach, namely, a smooth blade angle distribution is assumed from which the blade profile is generated. The axial distribution of the blade angle for the initial blade design is chosen to be

$$\frac{df}{dx} = (\tan\beta_2 - \tan\beta_1)\frac{e^{-\sigma x} - 1}{e^{-\sigma} - 1} + \tan\beta_1 \qquad (27)$$

In the present design, we choose $\sigma = 2$. In Eq. (27), the blade angle at the leading edge is set to be the freestream flow angle ($\beta_1 = 20$ deg, zero incidence condition), and the blade angle at the trailing edge is set to 0 deg with the intention that the flow leaves the blade axially ($\beta_2 = 0$ deg, blade deviation angle is assumed to be zero). The blade profile for this initial design is illustrated in Fig. 7 (circle symbol).

The flowfield about this blade was analyzed using the analysis mode of the code. Figure 8 (top part) illustrates the predicted Mach number contour about this initial design. This plot shows the presence of strong incident and reflected shocks appearing in the blade passage at the 85% axial chord location. Figure 9 (top part) shows the predicted entropy contour (normalized to the gas constant R). This figure confirms the presence of these oblique shocks, as indicated by the entropy increase behind the incident shock (formed by the convergence of the compression waves along the blade pressure

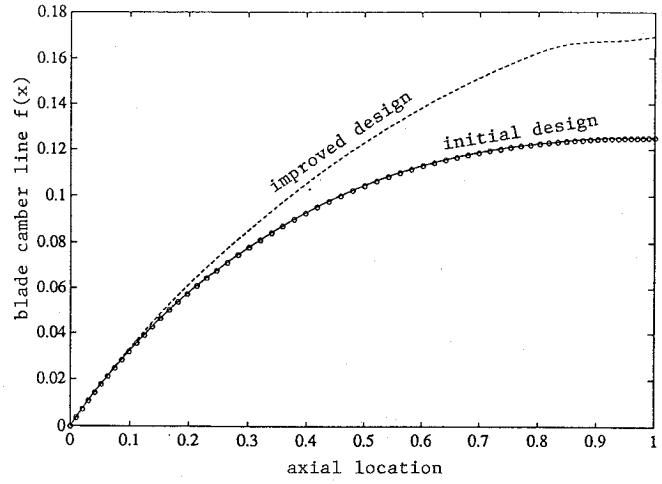

Fig. 7 Comparison of blade camber line: initial design/analysis mode is circle symbol, initial design/inverse mode is solid line, and improved design is dashed line.

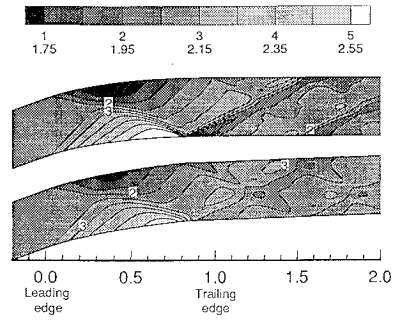

Fig. 8 Comparison of Mach number contour: initial design is at top of figure and improved design at bottom of figure.

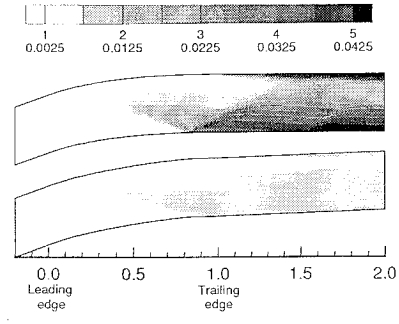

Fig. 9 Comparison of entropy contour: initial design at top of figure and improved design at bottom of figure.

surface near the leading-edge region) and the entropy increase behind the reflected shock (originated at the 85% axial chord location on the blade suction surface). Finally, Fig. 10 (circle symbol) shows the detailed blade surface Mach number distribution. It clearly indicates the presence of a strong shock at the 85% axial location and a reverse loading region between the 85% axial chord location and the blade trailing edge.

Next, a consistency study was carried out to reproduce this initial blade profile using the inverse mode of the computer code. This consistency study is rather challenging because this smooth blade profile corresponds to a flowfield with strong shocks in the blade passage. To carry out this consistency check, we need to determine the overall change in the normalized circumferential mass-averaged tangential velocity $\Delta\hat{V}_y$ of the initial blade design and the loading shape. These quantities can easily be extracted from the flow solutions obtained from the analysis mode. The overall change in the normalized circumferential mass-averaged tangential velocity $\Delta\hat{V}_y$ is calculated by the analysis mode to be −0.699. Figure 11 (solid line) illustrates the loading shape of the initial blade design. This figure shows the presence of 1) a rapid drop in the blade loading at the 85% chord

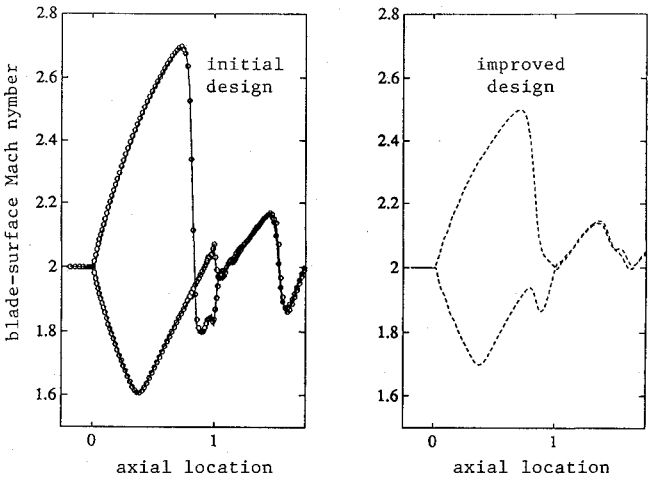

Fig. 10 Comparison of blade-surface Mach number: initial design/analysis mode is circle symbol, initial design/inverse mode is solid line, and improved design is dashed line.

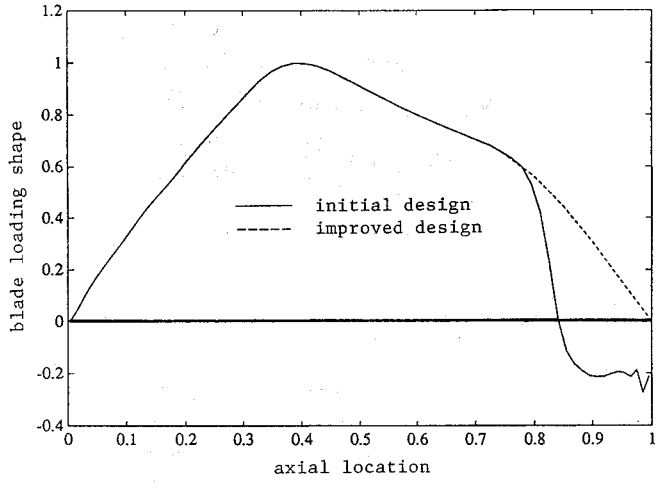

Fig. 11 Comparison of blade loading shape.

location and 2) a reverse (negative) loading region between the 85% chord location and the blade trailing edge. The loading shape given in Fig. 11 along with the computed value of $\Delta\hat{V}_y = -0.699$ are used to generate the $\hat{V}_y$ distribution for the inverse mode. Figure 7 shows very good agreement in the blade camber line distribution between the prescribed blade geometry (circle symbol) and the blade geometry computed by the inverse mode (solid line). Figure 10 illustrates an excellent comparison of the blade surface Mach number distribution between the analysis mode (circle symbol) and the inverse mode (solid line).

Finally, the proposed inverse method is used to improve this initial design which has at least two deficiencies. First, this blade profile overturns the flow by about 15% (i.e., the computed value of $\Delta\hat{V}_y$ is -0.699 compared to the designed value of -0.603). Second, the blade loading distribution shows the presence of an undesirable negative loading region (Fig. 11, solid line). To correct for these deficiencies, the inverse mode of the computer code is employed to obtain an improved blade design. The first deficiency is easily fixed since the inverse mode allows for a direct specification of $\Delta\hat{V}_y$. The second deficiency is accomplished by modifying the loading shape of the initial blade design so that the discontinuity at the 85% axial-chord location and the reverse loading region near the blade trailing edge are removed. Figure 11 (dashed line) shows the prescribed loading shape used to generate an improved blade design.

Figures 8 and 9 compare the Mach number and entropy contours between the initial design (top part) and the improved design (bottom part), respectively. Figure 10 compares the blade surface Mach number distribution between the initial design and the improved design. These figures clearly show that the improved design is superior to the initial design. Figure 9 shows that the improved design has weaker shocks than the initial design (the entropy rise is reduced by a factor of 4), and Fig. 10 shows that the improved design does not have a reverse loading region. It is interesting to note that both design have incident shocks along the suction surface at the 85% chord location, but the reflected shock is absent in the improved design. Figure 10 shows that the maximum Mach number in the blade passage is reduced. This is due to the fact that 1) the reverse blade loading is not present in the improved design and 2) the blade loading parameter $\Delta\hat{V}_y$ in the improved design is reduced from -0.699 to -0.603.

Figure 7 compares the initial and improved blade geometries. The most noticeable geometrical feature of the improved blade design is the presence of a shoulder (or a kink) around the 85% chord location. This shoulder produces a shock cancellation effect and results in the absence of the reflected shock in the improved blade design.

In terms of computational time, the analysis calculations for the subsonic-flow design with a 64×24 mesh take 5000 time steps to converge, whereas the inverse calculations take 10,000 time steps to converge. For the STF design, the analysis calculations with a 136×24 mesh take 1500 time steps to converge, whereas the inverse calculations take 2000 time steps to converge. These convergence rates are rather slow and are due to the fact that no convergence-acceleration technique is employed in these calculations. The CFL number used in these calculations is 2. In the inverse mode, the blade profile is updated every 10 time steps, and an under-relaxation value of 0.2 is used to update the blade camber line f.

VI. Summary

A three-dimensional inverse method for the design of turbomachine blades using existing time-marching techniques for the numerical solutions of the Euler equations is proposed. The general philosophy of this inverse method is based on the circulation method.[6–8] The primary difference between the present formulation and the earlier formulation is in the use of conservative variables rather than Clebsch variables. In this inverse method, the prescribed flow quantity is the circumferential mass-averaged tangential velocity distribution in the bladed region (or the blade loading), and the calculated geometrical quantity is the blade shape.

In this proposed inverse method, the presence of the blades are replaced by a periodic array of discrete body force field, which is shown to be related to the prescribed circumferential mass-averaged tangential velocity distribution. This discrete body force field is included in the numerical solution of the Euler equations via a pressure-jump boundary condition along the blade surfaces. A four-stage Runge–Kutta time-stepping scheme is used to march a finite volume formulation of the unsteady Euler equations to a steady-state solution.[17] The blade profile is periodically updated during this time-marching process using the flow-tangency conditions along the blade surfaces.

In this paper, the method is demonstrated for the design of infinitely thin cascaded blades ranging from the subsonic- to the supersonic-flow regimes. Examples presented include the design of compressor blades in irrotational and rotational flows, and supersonic throughflow fans with complex shock structures in the blade passage. Consistency checks for all of these design calculations are carried out using the analysis mode of the code.

As the purpose of this work is to introduce a newly developed three-dimensional inverse method for the aerodynamic design of turbomachinery blades, several assumptions are used in this initial study to facilitate the implementation of the theory. Specifically, the blades are assumed to be infinitely thin, and the flow is taken to be two dimensional and inviscid. With the use of these assumptions the method in its present form does not provide a useful design tool. It is important to recognize, however, that the purpose of the present study is not to develop another two-dimensional inverse method but rather to present the first step in the development of a fully three-dimensional and viscous inverse method. The extension of this method to three dimensions will be reported in Part 2. The theory formulated in this paper has been extended to handle blades with finite thickness[21] and we plan to incorporate the viscous body-force concept of Denton[16] to handle viscous effects.

Acknowledgments

This research was supported by the NASA Lewis Research Center under research Grant NAG3-1585 (David Miller, Technical Monitor) and the CASE Center at Syracuse University. The author would like to thank Jeffery Yokota at the NASA Lewis Research Center for his assistance in the development of the Euler analysis code.

References

[1]Giles, M. B., and Drela, M., "Two-Dimensional Transonic Aerodynamic Design Method," *AIAA Journal*, Vol. 25, 1987, pp. 1199–1205.

[2]Leonard, O., and Van den Braembussche, R. A., "Design Method for Subsonic and Transonic Cascade with Prescribed Mach Number Distribution," *Journal of Turbomachinery*, Vol. 114, 1992, pp. 553–560.

[3]Meauze, G., "An Inverse Time Marching Method for the Definition of Cascade Geometry," *Journal of Turbomachinery*, Vol. 11, 1982, pp. 650–656.

[4]Novak, R. A., and Haymann–Haber, "A Mixed-Flow Cascade Passage Design Procedure based on a Power Series Expansion," *Journal of Engineering for Gas Turbines and Power*, Vol. 105, 1983, pp. 231–242.

[5]Sanz, J. M., "Improved Design of Subcritical and Supercritical Cascades Using Complex Characteristics and Boundary-Layer Correction," *AIAA Journal*, Vol. 22, 1984, pp. 950–956.

[6]Dang, T. Q., and McCune, J. E., "A Three-Dimensional Design Method in Rotational Flow," *Proceedings of the International Conference on Inverse Design Concepts in Engineering Sciences (ICIDES)*, edited by G. S. Dulikravich, Univ. of Texas, Austin, TX, 1984, pp. 397–417.

[7]Hawthorne, W. R., Wang, C., Tan, C. S., and McCune, J. E., "Theory of Blade Design for Large Deflections: Part 1—Two-Dimensional Cascades," *Journal of Engineering for Gas Turbines and Power*, Vol. 106, 1984, pp. 346–353.

[8]Tan, C. S., Hawthorne, W. R., McCune, J. E., and Wang, C., "Theory of Blade Design for Large Deflections: Part II—Annular Cascades," *Journal of Engineering for Gas Turbines and Power*, Vol. 106, 1984, pp. 354–365.

[9]Dang, T. Q., "A Fully Three-Dimensional Inverse Method for Turbomachinery Blading in Transonic Flows," *Journal of Turbomachinery*, Vol. 115, 1993, pp. 354–361.

[10]Zangeneh, M., "Inviscid-Viscous Interaction Method for 3D Inverse Design of Centrifugal Impellers," ASME Paper 93-GT-103, 1993.

[11]Jiang, J., and Dang, T. Q., "Design Method for Turbomachine Blades with Finite Thickness by the Circulation Method," ASME Paper 94-GT-368, 1994.

[12]Yang, Y. L., Tan, C. S., and Hawthorne, W. R., "Aerodynamic Design of Turbomachinery Blading in Three-Dimensional Flow: An Application to Radial Inflow Turbines," *Journal of Engineering for Gas Turbines and Power*, Vol. 115, 1993, pp. 602–613.

[13]Borges, J. E., "A Three-Dimensional Inverse Method in Turbomachinery: Part 2—Experimental Verification," *Journal of Turbomachinery*, Vol. 112, 1990, pp. 355–361.

[14]Adamczyk, J. J., Celestina, M. L., Beach, T. A., and Barnett, M., "Simulation of 3D Viscous Flow Within a Multistage Turbine," *Journal of Turbomachinery*, Vol. 112, 1989, pp. 370–376.

[15]Dawes, W. N., "Toward Improved Throughflow Capability: The Use of Three-Dimensional Viscous Flow Solvers in a Multistage Environment," *Journal of Turbomachinery*, Vol. 114, 1992, pp. 8–17.

[16]Denton, J. D., "The Calculation of Three-Dimensional Viscous Flow Through Multistage Turbomachines," *Journal of Turbomachinery*, Vol. 114, 1992, pp. 18–26.

[17]Jameson, A., Schmidt, W., and Turkel, E., "Numerical Solution of the Euler Equations by Finite Volume Methods Using Runge–Kutta Time-Stepping Schemes," AIAA Paper 81-1259, 1981.

[18]Damle, S. V., Dang, T. Q., and Reddy, D. R., "Throughflow Method for Turbomachines Applicable for All Flow Regimes," ASME Paper 95-GT-395, 1995.

[19]Marsh, H., "A Digital Computer Program for the Through-Flow Fluid Mechanics in an Arbitrary Turbomachine Using a Matrix Method," ARC Rept R&M-3509, 1968.

[20]Smith, L. H., "Unducted Fan Aerodynamic Design," ASME Paper 87-GT-233, 1987.

[21]Dang, T., "Inverse Method for Turbomachine Blades Using Shock-Capturing Techniques," AIAA Paper 95-2465, 1995.

[22]Marble, F. E., "Three-Dimensional Flow in Turbomachines," *High Speed Aerodynamics and Jet Propulsion*, Vol. 10, Sec. C, Princeton Univ. Press, Princeton, NJ, 1964.

[23]Dang, T. Q., and Wang, T., "Design of Multi-Stage Turbomachinery Blading by the Circulation Method: Actuator Duct Limit," ASME Paper 92-GT-286, 1992.

[24]Whitfield, D. L., and Jameson, A., "Euler Equations Simulation of Propeller-Wing Interaction in Transonic Flow," *Journal of Aircraft*, Vol. 21, 1984, pp. 835–839.

[25]Dang, T. Q., and Isgro, V., "Inverse Method for Turbomachine Blades Using Existing Time-Marching Techniques," ASME Paper 94-GT-20, 1994.